Guiding center drift atoms[a]

S. G. Kuzmin and T. M. O'Neil[b]
Department of Physics, University of California at San Diego, La Jolla, California 92093

M. E. Glinsky
BHP Billiton Petroleum, Houston, Texas 77056

Very weakly bound electron-ion pairs in a strong magnetic field are called guiding center drift atoms, since the electron dynamics can be treated by guiding center drift theory. Over a wide range of weak binding, the coupled electron-ion dynamics for these systems is integrable. This paper discusses the dynamics, including the important cross magnetic field motion of an atom as a whole, in terms of the system constants of the motion. Since the dynamics is quasi-classical, quantum numbers are assigned using the Bohr–Sommerfeld rules. Antimatter versions of these guiding center drift atoms likely have been produced in recent experiments. © *2004 American Institute of Physics.* [DOI: 10.1063/1.1646158]

I. INTRODUCTION

This paper discusses the motion of a quasi-classical, weakly bound electron-ion pair in a strong magnetic field. The field is sufficiently strong that the electron cyclotron frequency is the largest of the dynamical frequencies and the cyclotron radius is the smallest of the length scales. In this limit, the rapid cyclotron motion can be averaged out, and the electron dynamics treated with guiding center drift theory. These weakly bound and strongly magnetized pairs are called guiding center drift atoms.[1]

Figure 1 shows a picture of the motion in a simple limit. The guiding center electron oscillates back and forth along the magnetic field in the Coulomb well of the ion, and more slowly $\vec{E} \times \vec{B}$ drifts around the ion. Let $z = z_e - z_i$ be the separation of the electron and ion along the direction of the magnetic field and $r = \sqrt{(x_e - x_i)^2 + (y_e - y_i)^2}$ the separation transverse to the field. For the case where the amplitude of the field aligned oscillations is not too large (i.e., $z_{max} \lesssim r$), the frequency of field aligned oscillations is approximately $\omega_z = \sqrt{e^2/(m_e r^3)}$ and the frequency of the $\vec{E} \times \vec{B}$ drift rotation is approximately $\omega_D = v_D/r = ce/(Br^3)$. These two frequencies are related to the electron cyclotron frequency, $\Omega_{ce} = eB/m_ec$ through the equation $\Omega_{ce} = \omega_z^2/\omega_D$. Thus, the requirement that the cyclotron frequency be larger than the other two frequencies imposes the ordering:

$$\Omega_{ce} \gg \omega_z \gg \omega_D. \tag{1}$$

The ordering is realized for sufficiently large separation (weak binding), that is, for $r \gg r_1 = (m_ec^2/B^2)^{1/3}$. This inequality is required for validity of our analysis.

Note that the the inequality implies not only that that the electron cyclotron frequency is large, but also that the electron cyclotron radius is small. We have in mind cases where the electron kinetic energy is smaller than or of order of the

electrostatic binding energy (i.e., $m_e v_e^2/2 \lesssim e^2/r$). The inequality $r \gg r_1$ then implies that $r_{ce} \equiv v_e/\Omega_{ce} \ll r$.

For r comparable to r_1 our guiding center analysis fails. All three frequencies in Eq. (1) are comparable, and the electron motion is chaotic.[2] For $r \ll r_1$, the cyclotron frequency is small compared to the Kepler frequency, and the electron motion is again integrable. In this case, one can think of the weakly bound pair as a high-n Rydberg atom with a Zeeman perturbation.[3]

The type of motion shown in Fig. 1, where the electron $\vec{E} \times \vec{B}$ drifts around the ion, occurs when $\omega_D > \Omega_{ci}$, v_i/r. Here, Ω_{ci} is the ion cyclotron frequency and v_i is the initial velocity of the ion transverse to the magnetic field. For this type of motion, the pair drifts across magnetic field with the transverse ion velocity $\vec{v}_i$ much like a neutral atom.

However, if the ion velocity is too large (i.e., $v_i/r \gg \omega_D$), the $\vec{E} \times \vec{B}$ drifting electron cannot keep up with the ion. The ion runs off and leaves the electron, which is effectively pinned to the magnetic field. More precisely, the ion moves in a large cyclotron orbit near the electron, the cyclotron motion being modified by electrostatic attraction to the electron. Of course, the electron oscillations back and forth along the magnetic field can become unbounded during large transverse excursions.

Figure 2 shows a kind of motion that can occur for relatively weak binding [i.e., $\Omega_{ci} > \omega_D$, or $r > r_2 = (m_i/m_e)^{1/3} r_1$]. The electron $\vec{E} \times \vec{B}$ drifts in the field of the ion, and the ion $\vec{E} \times \vec{B}$ drifts in the field of the electron. Together they form a so-called "drifting pair." In a drifting pair, the electron and ion move together across the magnetic field with the speed $v_D = ce/Br^2$.

The main purpose of this paper is to determine the character of the coupled electron-ion motion as a function of the constants of the motion. Fortunately, the Hamiltonian dynamics for the coupled system is integrable over a wide range of weak binding. The electron-ion system has six degrees of freedom so six constants of the motion are required for integrability. Four are exact constants: the Hamiltonian
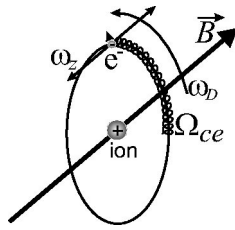

FIG. 1. Drawing of guiding center atom. In order of descending frequency, electron executes cyclotron motion, oscillates back and forth along a field line in the Coulomb well of the ion, $\vec{E}\times\vec{B}$ drifts around the ion.

and the three components of total momentum. The remaining two are approximate constants (adiabatic invariants) that result from two frequency separations. Because the electron cyclotron frequency is much larger than other dynamical frequencies the cyclotron action is a good adiabatic invariant. Use of guiding center drift variables automatically takes this constant into account and removes the cyclotron motion from the problem. Because the frequency of field aligned oscillations, ω_z, is much larger than the remaining dynamical frequencies (associated with cross field motion) the action associated with the field aligned motion is a good adiabatic invariant.

Inequality (1), which follows from the weak binding condition $r \gg r_1 = (m_e c^2/B^2)^{1/3}$, guarantees that the characteristic electron frequencies are ordered in accord with the assumed frequency separations. The frequencies that characterize the cross field ion motion (i.e., Ω_{ci} and v_i/r) also must be small compared to ω_z. The full frequency ordering is then

$$\Omega_{ce} \gg \omega_z \gg \omega_D, \Omega_{ci}, v_i/r. \tag{2}$$

The relative size of ω_D, Ω_{ci}, and v_i/r need not be specified; indeed, it is interplay between these frequencies that gives rise to the different types of motion discussed above. We will return to a detailed discussion of the frequency ordering later (see Sec. IV).

The analysis is carried out in a reference frame where the electric field vanishes. However, the effect of a uniform electric field directed transverse to the magnetic field can be included simply by shifting the transverse ion velocity [i.e., $\vec{v}_i(0) \to \vec{v}_i(0) - c\vec{E}\times\vec{B}/B^2$].

Antimatter versions of these guiding center drift atoms have likely been realized in recent experiments at the European Organization for Nuclear Research (CERN). The ATHENA[4] and ATRAP[5] collaborations have both reported success in producing cold antihydrogen atoms. The ATRAP collaboration measured binding energies of order meV,

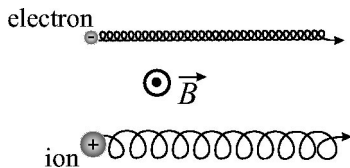FIG. 2. A kind of motion that occurs when electron and ion form a drifting pair.

which corresponds to $\bar{e}-\bar{p}$ separation of order 10^{-4} cm.[6] The magnetic field strength is 5 T, so the critical radius is $r_1 \equiv (m_e c^2/B^2)^{1/3} = 7 \times 10^{-6}$ cm. Thus, the separation is much larger than r_1, and the weakly bound pairs are guiding center atoms. The cyclotron frequency for the positron is about 100 times larger than the $\vec{E}\times\vec{B}$ drift frequency ω_D, and the cyclotron radius is about 100 times smaller than the separation. The ATHENA group did not measure binding energies, but the theory of three-body recombination, expected to be the dominant recombination process, suggests binding energies in the same range as those for ATRAP.

There has been much previous work on the coupled electron-ion system in a strong magnetic field. A difficulty is that a true separation of the center of mass motion (transverse to the magnetic field) and the internal motion is not possible. However, Avron, Herbst, and Simon[7] found an effective separation by introducing the transverse pseudomomentum and showing that it is a constant of motion. The influence of the transverse center of mass motion on the internal motion is then accounted for by a pseudopotential that depends on the eigenvalue of the pseudomomentum. More recently this effective separation was applied to the hydrogen atom[8] and positronium.[9]

In our classical analysis, the transverse pseudomomenta (P_X, P_Y) arise as two new momenta in a canonical transformation, and the pseudopotential enters the transformed Hamiltonian. Our analysis differs from the previous work in that the Hamiltonian is simplified by the use of frequency ordering (2), which relies on both strong magnetic field and weak binding. Introduction of the cyclotron action and of the action for the field aligned bounce motion effectively averages the Hamiltonian over the rapid cyclotron and bounce motions, removing two degrees of freedom at the outset. In the language of atomic physics, a double Born–Oppenheimer approximation is used. The remaining transverse dynamics is always integrable, and a transverse action can be introduced. Since the Hamiltonian is expressed as a function of the cyclotron action, bounce action, and transverse action, a general expression for the quantum energy levels can be obtained using the Bohr–Sommerfeld quantization rules. Of course the assumption of weak binding justifies the quasi-classical approximation—with the possible exception of the cyclotron motion, as will be discussed. We will compare general quasi-classical predictions for energy levels to predictions from quantum calculations in limiting cases.

Much of the previous work has focused on an "outer well" that exists in the pseudopotential for sufficiently large pseudomomentum and the consequent "delocalized atomic states."[7,8] From the prospective of guiding center drift theory, these delocalized states are simply an electron and ion $\vec{E}\times\vec{B}$ drifting in each other's field as shown in Fig. 2. The criterion for the existence of the outer well in the exact pseudopotential is that the scaled pseudomomentum be larger than a certain value, $\tilde{P} \geq \tilde{P}_c = 3/4^{1/3}$.[8] The reader may wish to skip ahead to Eq. (18) for the definition of $\tilde{P}$. This is a necessary criterion for the existence of the delocalized states. Working with the bounce averaged pseudopotential,

we find a necessary and sufficient criterion for the delocalized states, $\tilde{P} > \tilde{P}(\tilde{I}_z)$, where $\tilde{I}_z$ is the scaled bounce action. As we will see, $\tilde{P}_c(\tilde{I}_z)$ reduces to $\tilde{P}_c = 3/4^{1/3}$ for $\tilde{I}_z = 0$.

The name "guiding center drift atom" was coined in Ref. 1. Indeed, a version of Fig. 1 appears in Ref. 1. Likewise, the possibility of "$\mathbf{E} \times \mathbf{B}$ drifting pairs" and "runaway ions" was discussed. However, Ref. 1 did not exploit the integrability of the Hamiltonian to discuss the atom dynamics as a function of the constants of the motion, which is the principle focus of this paper. Rather, anticipating the programs to produce antihydrogen,[4,5] Ref. 1 extended the theory of three-body recombination to the case of guiding center drift atoms. The theory treated the simple case where the ion (or antiproton) is stationary. The general characterization of atom dynamics developed here is a prerequisite to an analysis of three-body recombination that takes into account ion motion.

II. HAMILTONIAN AND CONSTANTS OF MOTION

We consider a uniform magnetic field $\vec{B} = \hat{z}B$ represented by the vector potential $\vec{A} = Bx\hat{y}$. The external electric field is chosen to be zero. The Hamiltonian for a guiding center drift electron and an ion that interact electrostatically and move in the magnetic field is given by

$$
\begin{aligned}
H = & I_{ce}\Omega_{ce} + \frac{1}{2m_e}p_{ze}^2 + \frac{1}{2m_i}p_{xi}^2 \\
& + \frac{1}{2m_i}\left(p_{yi}^2 - \frac{e}{c}Bx_i\right)^2 + \frac{1}{2m_i}p_{zi}^2 \\
& - \frac{e^2}{\sqrt{\left(x_i + \dfrac{c}{eB}p_{ye}\right)^2 + (y_i - y_e)^2 + (z_i - z_e)^2}}.
\end{aligned}
\tag{3}
$$

Here, the first two terms are the electron kinetic energy, where Ω_{ce} is the cyclotron frequency and I_{ce} is the cyclotron action. The product is the kinetic energy associated with velocity components transverse to the magnetic field. Since I_{ce} is a good adiabatic invariant and Ω_{ce} is constant (for a uniform magnetic field), the product $I_{ce}\Omega_{ce}$ is constant and does not influence the dynamics of the remaining variables. The quantities x_i, y_i, z_i, z_e, and y_e are ion and electron coordinates; and the momenta conjugate to these coordinates are given by

$$p_{xi} = m_i\dot{x}_i,$$

$$p_{yi} = m_i\dot{y}_i + \frac{eB}{c}x_i,$$

$$p_{zi} = m_i\dot{z}_i, \tag{4}$$

$$p_{ye} = -\frac{eB}{c}x_e,$$

$$p_{ze} = m_e\dot{z}_e.$$

The electron position transverse to the field is specified by $(y_e, p_{ye} = -eBx_e/c)$, and $x_e, p_{xe} = m_e\dot{x}_e$ are removed from

the dynamics. The removal of one degree of freedom results from averaging out the rapid cyclotron motion.

Let us make a canonical transformation to a new set of variables

$$P_X = p_{xi} + \frac{eB}{c}(y_e - y_i), \quad X = \frac{c}{eB}(p_{yi} + p_{ye}) + x_i,$$

$$P_Y = p_{yi} + p_{ye}, \quad Y = \frac{c}{eB}p_{xi} + y_e,$$

$$P_Z = p_{zi} + p_{ze}, \quad Z = \frac{m_i z_i + m_e z_e}{m_i + m_e}, \tag{5}$$

$$p_y = \frac{eB}{c}x_i + p_{ye}, \quad y = y_e - y_i,$$

$$p_z = \frac{m_i p_{ze} - m_e p_{zi}}{m_i + m_e}, \quad z = z_e - z_i.$$

To verify that the transformation is canonical, one can check that Poisson brackets are equal to unity for conjugate variables and vanish otherwise. The Hamiltonian in the new variables has the form

$$
\begin{aligned}
H = & I_{ce}\Omega_{ce} + \frac{1}{2m_i}\left(P_X - \frac{eB}{c}y\right)^2 + \frac{1}{2m_i}(P_Y - p_y)^2 \\
& + \frac{1}{2M}P_Z^2 + \frac{1}{2\mu}p_z^2 - \frac{e^2}{\sqrt{\left(\dfrac{c}{eB}p_y\right)^2 + y^2 + z^2}},
\end{aligned}
\tag{6}
$$

where $M = m_i + m_e$, and $\mu = m_i m_e/(m_i + m_e)$ are total and reduced mass, respectively. Since the mass ratio is assumed to be small ($m_e/m_i \ll 1$), we set $M \simeq m_i$ and $\mu \simeq m_e$ in the subsequent analysis. The Hamiltonian is independent of t, X, Y, and Z, so H, P_X, P_Y, and P_Z are constants of the motion. We work in a frame where P_Z is zero (the center of mass frame), and we orient the coordinates axis so that P_X is zero. This involves no loss of generality. In the Hamiltonian, the sum of the two terms that govern the z motion are the binding energy

$$H_z = \frac{1}{2\mu}p_z^2 - \frac{e^2}{\sqrt{r^2 + z^2}}, \tag{7}$$

where

$$\vec{r} = \left(-\frac{c}{eB}p_y, \ y, \ 0\right) \equiv (x_e - x_i, \ y_e - y_i, \ 0). \tag{8}$$

The electron kinetic energy associated with velocity components transverse to the magnetic field is bound up in the cyclotron action, I_{ce}. For a bound electron-ion pair, H_z is negative.

In previous work[7–9] the momentum $\vec{P} = (P_X, P_Y)$ is called the pseudomomentum. Likewise, the second two terms in Hamiltonian (6), which are the transverse kinetic energy of the ion, are thought of as a pseudopotential for the transverse internal motion [i.e., for (y, p_y)].

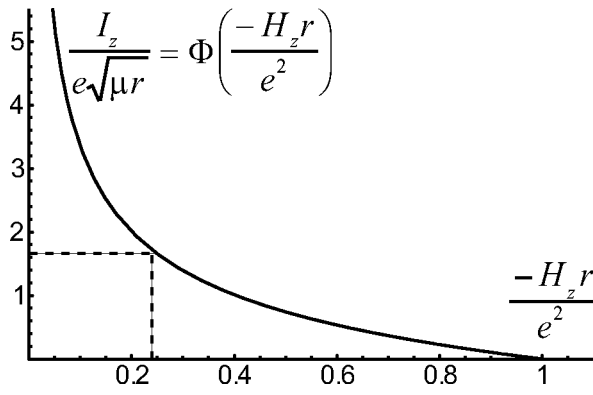One further constant is required for integrability, and it is given by the bounce action for the z motion,

FIG. 3. Graphical solution of Eq. (9). Knowing I_z and r, one can find $H_z(r,I_z)$.

$$I_z = \frac{1}{2\pi} \oint p_z\, dz = e\sqrt{\mu r}\ \Phi\left(\frac{-H_z r}{e^2}\right), \qquad (9)$$

which is a good adiabatic invariant for sufficiently large bounce frequency. In carrying out the integral, H_z and r are held constant. The function $\Phi(\xi)$ is given by

$$\Phi(\xi) = \frac{2\sqrt{2}}{\pi\sqrt{\xi}} \int_{\xi}^{1} \sqrt{\frac{q - q^2}{q^2 - \xi^2}}\, dq$$

$$= \frac{2\sqrt{2}}{\pi\xi\sqrt{1+\xi}} \left[-\xi(\xi+1)E\left(\frac{\xi-1}{\xi+1}\right) \right.$$

$$\left. + \xi K\left(\frac{\xi-1}{\xi+1}\right) + \Pi\left(\frac{\xi-1}{\xi}, \frac{\xi-1}{\xi+1}\right) \right], \qquad (10)$$

where E, K, and Π are the complete elliptic integrals and the argument of Φ is $\xi = -H_z r/e^2$. For future reference we note that $\xi = r/\sqrt{z_{max}^2 + r^2}$, where z_{max} is the amplitude of the field aligned oscillations. Figure 3 shows a plot of $\Phi(\xi)$ on the interval [0,1]. The figure also shows a graphical inversion to obtain H_z as a function of I_z and r. Formally, we write the inversion as

$$H_z(r,I_z) = -\frac{e^2}{r} \Phi^{-1}\left(\frac{I_z}{e\sqrt{m_e r}}\right). \qquad (11)$$

When $\xi = -H_z r/e^2$ is close to 1, the amplitude of axial electron oscillations in the Coulomb well is small compared to r, and the potential is approximately harmonic. In this case $\Phi(\xi)$ can be approximated by linear dependence:

$$\Phi(\xi) \simeq 1 - \xi, \qquad (12)$$

and H_z and I_z are related as

$$H_z(r,I_z) \simeq -\frac{e^2}{r} + I_z\omega_z, \qquad (13)$$

where $\omega_z^2 = e^2/(\mu r^3)$. As one expects, the Coulomb potential energy, $-e^2/r$, is corrected by the addition of a small term $I_z\omega_z$, the oscillation energy in a harmonic well.

Analytic treatment also is possible when the amplitude of oscillation is near the limit allowed by binding (i.e., $\xi = -H_z r/e^2 \ll 1$). One can approximate the function $\Phi(\xi)$ with an asymptotic series

$$\Phi(\xi) \simeq \sqrt{\frac{2}{\xi}} - \frac{4\sqrt{2}}{\pi}[E(-1) - K(-1)] - \cdots. \qquad (14)$$

Using the first two terms in this series yields the approximate expression

$$H_z(r,I_z) \simeq -\frac{2\mu e^4}{\left(I_z + \frac{4}{\pi}[E(-1) - K(-1)]e\sqrt{2\mu r}\right)^2}. \qquad (15)$$

We can see from (15) that for finite bounce oscillations ($I_z \neq 0$), the electron binding energy H_z has the minimum possible value $H_z = -2\mu e^4/I_z^2$. If the electron-ion transverse separation were slowly reduced, the binding energy would not go to minus infinity. Note that expression (15) is only valid for I_z such that $I_z \gg e\sqrt{\mu r}$.

Substituting Eqs. (7) and (11) plus the choices $P_X = P_Z = 0$ into Hamiltonian (6) yields an implicit equation for the phase space trajectory [i.e., for $p_y(y)$],

$$H = I_{ce}\Omega_{ce} + \frac{1}{2}m_i\Omega_{ci}y^2 + \frac{1}{2m_i}(P_Y - p_y)^2$$

$$- \frac{e^2}{r}\Phi^{-1}\left(\frac{I_z}{e\sqrt{m_e r}}\right), \qquad (16)$$

where r is related to y and p_y through Eq. (8). The trajectory is specified by the values of H, P, and I_z. With the additional input of an initial point along the trajectory [e.g., $y(t=0)$ or $p_y(t=0)$], the Hamiltonian equations of motion can be solved to find $y(t)$ and $p_y(t)$. Given this solution, the coordinates of the electron and ion are determined separately by

$$\frac{dx_i}{dt} = -\frac{eB}{m_i c}y(t), \qquad \frac{dy_i}{dt} = \frac{P_Y}{m_i} - \frac{p_y(t)}{m_i},$$

$$\frac{dp_{ye}}{dt} = -\frac{\partial H_z(r,I_z)}{\partial y}, \qquad \frac{dy_e}{dt} = \frac{\partial H_z(r,I_z)}{\partial p_y}. \qquad (17)$$

These equations follow from Eqs. (4) and (5) and the choice $P_X = 0$.

III. PHASE TRAJECTORIES IN SCALED VARIABLES

The dependence of the phase trajectories on parameters such as e and B can be buried in scaled variables. Using $r_2 = (m_i c^2/B^2)^{1/3} = (m_i/m_e)^{1/3} r_1$, Ω_{ci}^{-1}, and m_i as the units of length, time, and mass yields the scaled variables

$$\tilde{P} = P_Y/(m_i\Omega_{ci}r_2),$$

$$\tilde{y} = y/r_2,$$

$$\tilde{p}_y = p_y/(m_i\Omega_{ci}r_2),$$

$$\tilde{H} = H/(m_i\Omega_{ci}^2 r_2^2), \qquad (18)$$

$$\tilde{H}_z = H_z/(m_i\Omega_{ci}^2 r_2^2),$$

$$\tilde{I}_z = I_z/(m_i\Omega_{ci}r_2^2),$$

$$\widetilde{I}_{ce} = I_{ce}/(m_i \Omega_{ci} r_2^2),$$

and the scaled Hamiltonian

$$\widetilde{H} = \frac{m_i}{m_e}\widetilde{I}_{ce} + \frac{1}{2}(\widetilde{P} - \widetilde{p}_y)^2 + \frac{1}{2}\widetilde{y}^2 - \frac{1}{\widetilde{r}}\Phi^{-1}\left(\sqrt{\frac{m_i}{m_e}}\frac{\widetilde{I}_z}{\sqrt{\widetilde{r}}}\right), \tag{19}$$

where the $\widetilde{r} = \widetilde{x}^2 + \widetilde{y}^2$ and $\widetilde{x} = -\widetilde{p}_y$. Likewise, Eq. (17) takes the scaled form

$$\frac{d\widetilde{x}_i}{d\widetilde{t}} = -\widetilde{y}(\widetilde{t}), \quad \frac{d\widetilde{y}_i}{d\widetilde{t}} = \widetilde{P} - \widetilde{p}_y(\widetilde{t}),$$

$$\frac{d\widetilde{p}_{ye}}{d\widetilde{t}} = -\frac{\partial \widetilde{H}_z}{\partial \widetilde{y}}, \quad \frac{d\widetilde{y}_e}{d\widetilde{t}} = \frac{\partial \widetilde{H}_z}{\partial \widetilde{p}_y}, \tag{20}$$

where $\widetilde{H}_z$ is the last term in Hamiltonian (19) and the scaled time is $\widetilde{t} = t\Omega_{ci}$.

We have in mind cases where the scaled variables $\widetilde{P}$, $\widetilde{y}$, and $\widetilde{p}_y = -\widetilde{x}$ are all of order unity, but $\widetilde{I}_z$ is of order $\sqrt{m_e/m_i}$. The product $\sqrt{m_i/m_e}\widetilde{I}_z$, which enters the last term is then of order unity. In the following discussion of trajectories we will specify the value of the product $\sqrt{m_i/m_e}\widetilde{I}_z$. The significance of the factor $\sqrt{m_i/m_e}$ will be apparent in the next section where we evaluate frequencies as derivatives of $\widetilde{H}$ with respect to actions.

For the simple case $\sqrt{m_i/m_e}\widetilde{I}_z = 0$, Hamiltonian (19) reduces to the form

$$\widetilde{H} = \frac{1}{2}(\widetilde{P} - \widetilde{p}_y)^2 + \frac{1}{2}\widetilde{y}^2 - \frac{1}{\sqrt{\widetilde{p}_y^2 + \widetilde{y}^2}}, \tag{21}$$

where the constant term $(m_i/m_e)\widetilde{I}_{ce}$ has been dropped. Phase trajectories in this case depend only on two parameters, $\widetilde{H}$ and $\widetilde{P}$. Depending on the value of $\widetilde{P}$ there can be different types of phase portraits. Three different cases are presented in Figs. 4–6.

Figure 4(a) shows the phase trajectories for the case where $\widetilde{P} = 2.5$ is greater than a certain critical value, $\widetilde{P}_c = 3/4^{1/3}$. Figure 4(b) shows a plot of $\widetilde{H}(\widetilde{y}=0,\widetilde{p}_y,\widetilde{P})$. One can see that $\widetilde{H}$ has two minima, one at $(\widetilde{y},\widetilde{p}_y) = (0,0)$ (where $\widetilde{H} \to -\infty$), and another at $\widetilde{y} = 0$ and finite $\widetilde{p}_y$.

There are three classes of trajectories divided by the separatrix shown as the dashed curve in Fig. 4(a). For the first class, the trajectories encircle the minimum at $(\widetilde{y},\widetilde{p}_y) = (0,0)$. For the second class, the trajectories encircle the minimum at $\widetilde{y} = 0$ and finite $\widetilde{p}_y$. For the third class, the trajectories encircle both minima. We will now describe the prototypical motion for each class in an extreme limit where the motion is simple. Of course, for a trajectory not near one of these limits, say, a trajectory near the separatrix dividing two classes, the motion is a complicated mix of the two limits.

For the trajectories encircling the minimum at $(\widetilde{y},\widetilde{p}_y) = (0,0)$ with small $\widetilde{r} = \sqrt{\widetilde{y}^2 + \widetilde{p}_y^2}$, the electron $\vec{E} \times \vec{B}$ drifts around the ion as shown in Fig. 1. This kind of motion re-
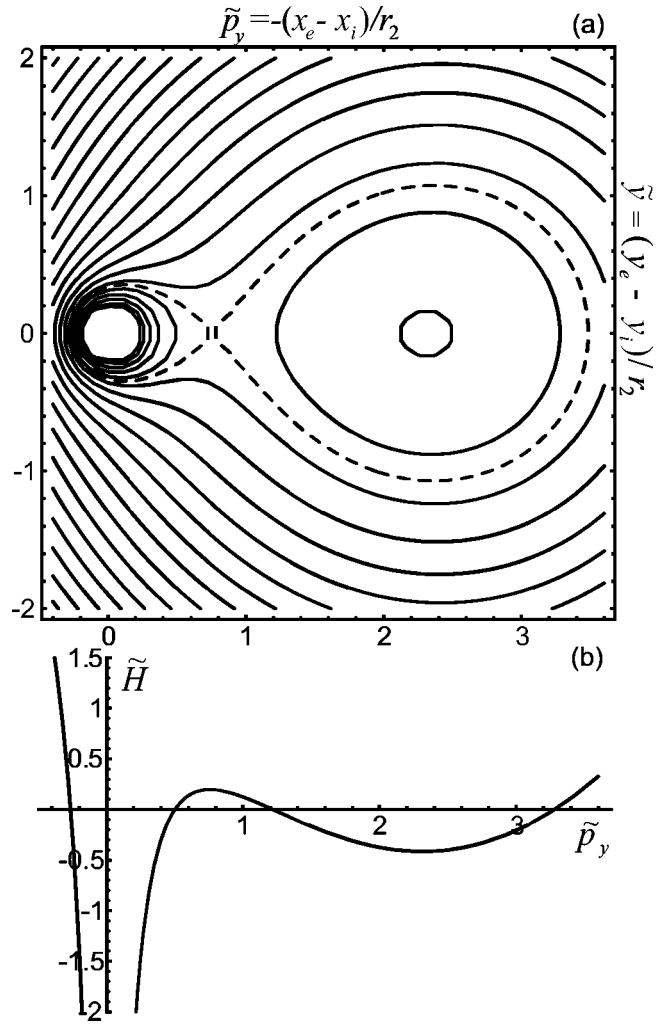

FIG. 4. (a) Phase trajectories for the case when $\widetilde{I}_z = 0$, $\widetilde{P} = 2.5 > \widetilde{P}_c$; (b) section of $\widetilde{H}(\widetilde{p}_y,\widetilde{y},\widetilde{P})$ over the plane $\widetilde{y} = 0$.

quires the electron $\vec{E} \times \vec{B}$ drift velocity to be large compared to the ion velocity. From Eq. (20), we see that for $\widetilde{r} \ll 1$ and $\widetilde{P}$ order unity or larger, the ion velocity is approximately $\widetilde{v}_i \equiv \sqrt{(d\widetilde{x}_i/d\widetilde{t})^2 + (d\widetilde{y}_i/d\widetilde{t})^2} \simeq \widetilde{P}$ and the velocity $\widetilde{v}_e \equiv \sqrt{(d\widetilde{y}_e/d\widetilde{t})^2 + (d\widetilde{p}_{ye}/d\widetilde{t})^2} \simeq 1/\widetilde{r}^2$. Thus, the ratio

$$\frac{\widetilde{v}_i}{\widetilde{v}_e} \simeq \widetilde{P}\widetilde{r}^2 \tag{22}$$

is small for sufficiently small $\widetilde{r}$. The bound electron-ion pair moves across the magnetic field with a velocity that is nearly equal to the initial ion velocity,

$$\left\langle \frac{d\widetilde{x}_i}{d\widetilde{t}} \right\rangle = -\langle \widetilde{y} \rangle = 0,$$

$$\left\langle \frac{d\widetilde{y}_i}{d\widetilde{t}} \right\rangle = \widetilde{P} - \langle \widetilde{p}_y \rangle \simeq \widetilde{P} \simeq \frac{v_{yi}(0)}{r_2\Omega_{ci}}. \tag{23}$$

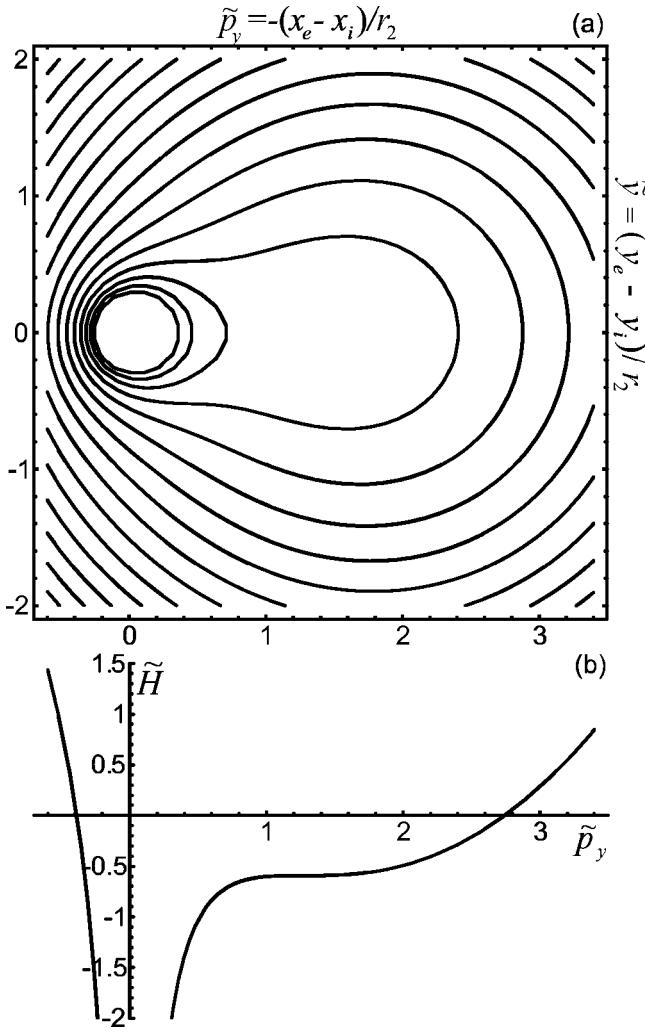Here, the angular brackets indicate an average over the rapid $\vec{E} \times \vec{B}$ drift motion of the electron.

$$\tilde{p}_y = -(x_e - x_i)/r_2 \qquad \text{(a)}$$

$$\tilde{y} = (y_e - y_i)/r_2$$

$$\tilde{H} \qquad \text{(b)}$$

$$\tilde{p}_y$$

FIG. 5. Same as in Fig. 4 but $\tilde{P} = 3/4^{1/3} = \tilde{P}_c$.

$$\tilde{p}_y = -(x_e - x_i)/r_2 \qquad \text{(a)}$$

$$\tilde{y} = (y_e - y_i)/r_2$$

$$\tilde{H} \qquad \text{(b)}$$

$$\tilde{p}_y$$

FIG. 6. Same as in Fig. 4 but $\tilde{P} = 1.5 < \tilde{P}_c$.

For the trajectories that encircle the second minimum tightly, the electron and ion $\vec{E} \times \vec{B}$ drift together as shown in Fig. 2. According to Eq. (20) the electron and ion velocities are given by

$$\frac{d\tilde{y}_e}{d\tilde{t}} \simeq \frac{\tilde{p}_{ym}}{|\tilde{p}_{ym}|^3}, \qquad \frac{d\tilde{y}_i}{d\tilde{t}} \simeq \tilde{P} - \tilde{p}_{ym}, \qquad (24)$$

where $\tilde{p}_{ym}$ is the location of the minimum. Note that $d\tilde{x}_i/d\tilde{t}$ and $d\tilde{p}_{ye}/d\tilde{t}$ are both nearly zero. The minimum is the root of

$$0 = \frac{d\tilde{H}}{d\tilde{p}_y} = -(\tilde{P} - \tilde{p}_y) + \frac{\tilde{p}_y}{|\tilde{p}_y|^3}, \qquad (25)$$

so the electron and ion velocities are equal, both given by the $\vec{E} \times \vec{B}$ formula.

For the large circular trajectories (i.e., $\tilde{r} \gg 1$), the ion executes a cyclotron orbit in the vicinity of the electron. The electron $\vec{E} \times \vec{B}$ drift velocity is small compared to the ion velocity for these large $\tilde{r}$ trajectories.

If the value of the transverse momentum $\tilde{P}$ is decreased, the minimum at $\tilde{y} = 0$ and finite $\tilde{p}_y$ disappears. Figures 5(a)
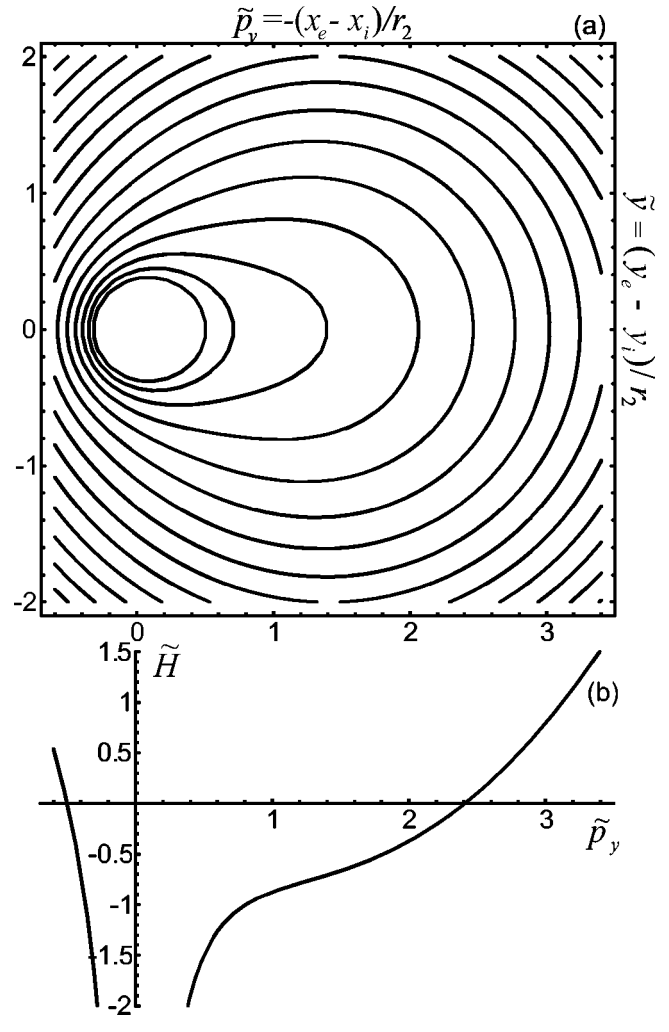
and 5(b) show the the trajectories and Hamiltonian for the critical value $\tilde{P}_c = 3/4^{1/3}$. Figures 6(a) and 6(b) show the same for a sub-critical value, $\tilde{P} = 1.5 < \tilde{P}_c$. One can see that $\vec{E} \times \vec{B}$ drifting pairs [see Fig. 2] are no longer possible.

For the general case where $\sqrt{m_i/m_e}\tilde{I}_z \neq 0$, Hamiltonian (19) must be used to plot the trajectories. An important difference is that the binding energy

$$\tilde{H}_z = -\frac{1}{\tilde{r}}\Phi^{-1}\left(\sqrt{\frac{m_i}{m_e}}\frac{\tilde{I}_z}{\sqrt{\tilde{r}}}\right) \qquad (26)$$

does not diverge at $\tilde{r} = 0$ when $\sqrt{m_i/m_e}\tilde{I}_z$ is non-zero. This is to be expected since the potential $-1/\sqrt{\tilde{z}^2 + \tilde{r}^2}$ does not diverge at $\tilde{r} = 0$ for finite $\tilde{z}$. As mentioned earlier [see Eq. (15)], $\tilde{H}_z$ reaches the minimum value $-2/(\sqrt{m_i/m_e}\tilde{I}_z)^2$ as $\tilde{r}$ approaches zero. Plots of $\tilde{H}_z$ vs $\tilde{r}$ for various values of $\sqrt{m_i/m_e}\tilde{I}_z$ are shown in Fig. 7.

The phase trajectories for non-zero $\sqrt{m_i/m_e}\tilde{I}_z$ are qualitatively like those shown in Figs. 4–6. However, the critical value of $\tilde{P}$, signifying the loss of the separatrix, is a slowly decreasing function of $\sqrt{m_i/m_e}\tilde{I}_z$. Figure 8 shows a plot of $\tilde{P}_c(\sqrt{m_i/m_e}\tilde{I}_z)$ for $\sqrt{m_i/m_e}\tilde{I}_z$ ranging from 0 to 1. As illus-
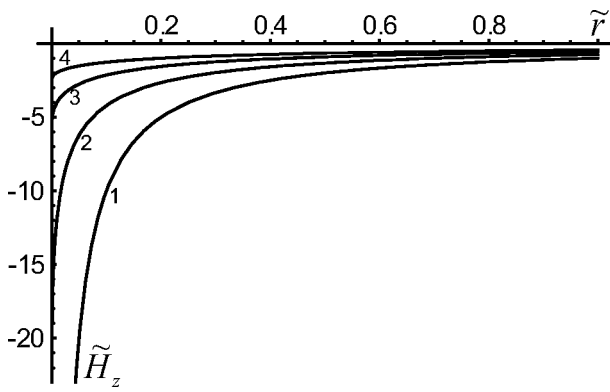
FIG. 7. Plot of binding energy $\tilde{H}_z$ at different values of $\sqrt{m_i/m_e}\tilde{I}_z$. (1) $\sqrt{m_i/m_e}\tilde{I}_z=0$ (in this case $\tilde{H}_z=-1/\tilde{r}$); (2) $\sqrt{m_i/m_e}\tilde{I}_z=0.3$; (3) $\sqrt{m_i/m_e}\tilde{I}_z=0.6$; (4) $\sqrt{m_i/m_e}\tilde{I}_z=0.9$.

trations, Figs. 9 and 10 show phase space trajectories for the same values of $\tilde{P}$ [i.e., $\tilde{P}=1.5$] but for different values of $\sqrt{m_i/m_e}\tilde{I}_z$ (i.e., $\sqrt{m_i/m_e}\tilde{I}_z=0.3$ and $\sqrt{m_i/m_e}\tilde{I}_z=0.9$). In Fig. 9 there is no separatrix, since $\tilde{P}=1.5$ is below the critical value $\tilde{P}_c(\sqrt{m_i/m_e}\tilde{I}_z=0.3)\simeq1.64$; whereas in Fig. 10 there is a separatrix, since $\tilde{P}=1.5$ is above the critical value $\tilde{P}_c(\sqrt{m_i/m_e}\tilde{I}_z=0.9)\simeq1.15$.

IV. FREQUENCY SEPARATION AND THE ADIABATIC INVARIANTS

In this section, we examine the frequency separation required for validity of the adiabatic invariants. For a case where the separation is well satisfied, we will see that a solution of the full equations of motion, including the electron cyclotron motion, compares well to the corresponding trajectory obtained using constancy of the adiabatic invariants. For a case where the separation is not satisfied, the numerical solution of the full equations of motion exhibits breakdown of the adiabatic invariants and apparent chaotic motion.

The frequency separation can be understood as a consequence of the large mass ratio $m_i/m_e\gg1$. In Hamiltonian (19), suppose that the cross field scaled variables are all of order unity [i.e., $\tilde{P}$, $\tilde{y}$, $\tilde{p}_y\sim O(1)$] and that $\sqrt{m_i/m_e}\tilde{I}_z$,

FIG. 9. Phase portrait of the system for the case when $\tilde{P}=1.5$, $\sqrt{m_i/m_e}\tilde{I}_z=0.3$; the radius of dashed circle in the center is equal to $\tilde{r}_1=r_1/r_2$.

$(m_i/m_e)\tilde{I}_c\sim O(1)$. The scale cyclotron frequency is $\partial\tilde{H}/\partial\tilde{I}_c=m_i/m_e$, the scaled frequency of field aligned oscillations is $\partial\tilde{H}/\partial\tilde{I}_z\sim O(\sqrt{m_i/m_e})$ and the scaled cross field frequencies are of order unity. Thus, the three classes of frequencies in inequality (2) are ordered as $m_i/m_e\gg\sqrt{m_i/m_e}\gg1$.

Let us look at the field aligned oscillations more closely. For arbitrary $\xi=\tilde{r}/\sqrt{\tilde{r}^2+\tilde{z}_{max}^2}$, the scaled frequency is given by

$$\frac{\partial\tilde{H}_z}{\partial\tilde{I}_z}=\sqrt{\frac{m_i}{m_e}}\frac{1}{\tilde{r}^{3/2}}\frac{1}{-\Phi'(\xi)}=\sqrt{\frac{m_i}{m_e}}\left(\frac{\xi}{\tilde{r}}\right)^{3/2}\Theta(\xi),\quad(27)$$
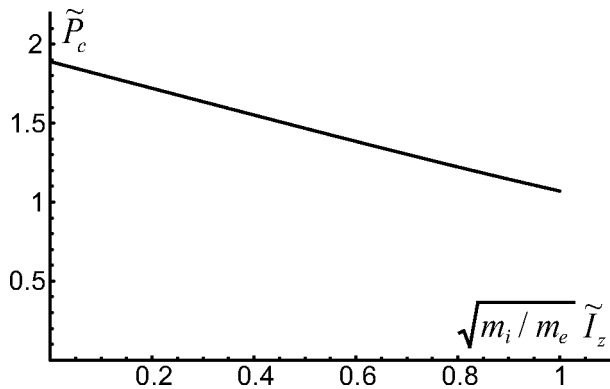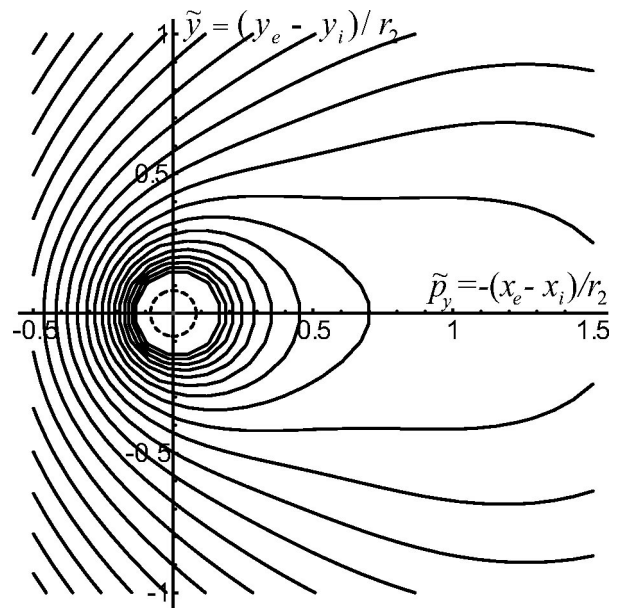

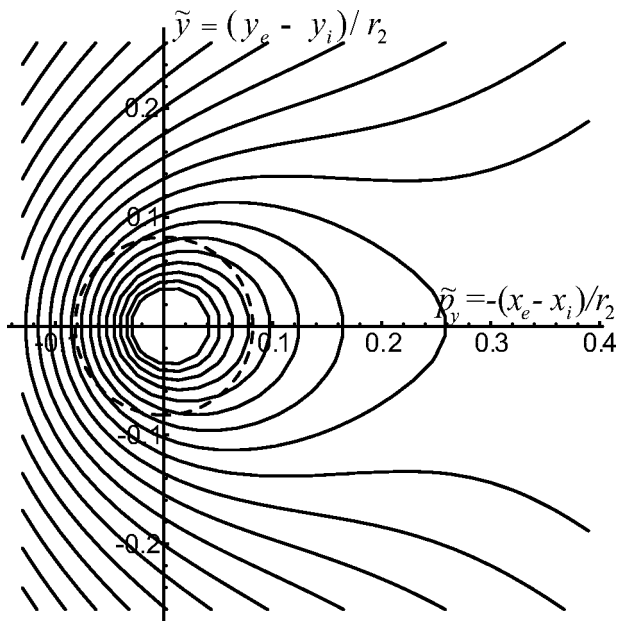FIG. 8. Plot of $\tilde{P}_c(\tilde{I}_z)$.

FIG. 10. Phase portrait of the system for the case when $\tilde{P}=1.5$, $\sqrt{m_i/m_e}\tilde{I}_z=0.9$; the radius of dashed circle in the center is equal to $\tilde{r}_1$.

Phys. Plasmas, Vol. 11, No. 5, May 2004
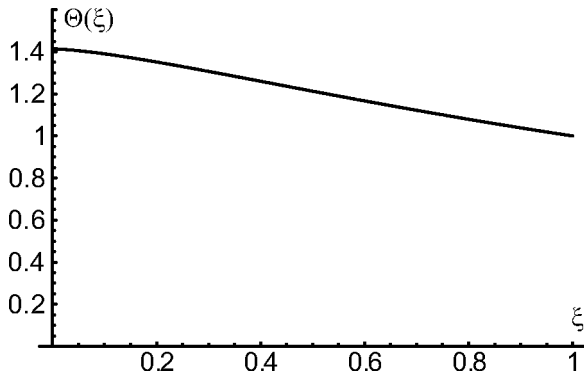
Guiding center drift atoms   2389

FIG. 11. Plot of function $\Theta(\xi)$.

where the function $\Theta(\xi)$ is plotted in Fig. 11. Since $\Theta(\xi)$ is unity to within a factor of $\sqrt{2}$ over the full range of ξ values (i.e., $0 \leq \xi \leq 1$), the scaled frequency is approximately

$$\frac{\partial \tilde{H}_z}{\partial \tilde{I}_z} \simeq \sqrt{\frac{m_i}{m_e}} \left(\frac{\xi}{\tilde{r}}\right)^{3/2} = \sqrt{\frac{m_i}{m_e}} \frac{1}{(\tilde{r}^2 + \tilde{z}_{max}^2)^{3/4}} \quad (28)$$

for arbitrary $\tilde{z}_{max}$. As expected, the maximum $\partial \tilde{H}_z / \partial \tilde{I}_z|_{max} = \sqrt{m_i/m_e}\tilde{r}^{-3/2}$, occurs for $z_{max}=0$.

In Sec. I we required that

$$\frac{\partial \tilde{H}_z}{\partial \tilde{I}_c} = \frac{m_i}{m_e} \frac{\partial \tilde{H}_z}{\partial \tilde{I}_z}\bigg|_{max} = \sqrt{\frac{m_i}{m_e}} \frac{1}{\tilde{r}^{3/2}}, \quad (29)$$

which can be written as the requirement $r \gg r_2(m_e/m_i)^{1/3} = r_1$. Since $\partial \tilde{H}_z / \partial \tilde{I}_z$ is much smaller than $\partial \tilde{H}_z / \partial \tilde{I}_z|_{max}$ for $\tilde{z}_{max} \gg \tilde{r}$, one might think that requirement (29) is overly restrictive. However, there are high frequency components in the motion that are of order of $\sqrt{m_i/m_e}\tilde{r}^{-3/2}$. These high frequency components are associated with the passage of the electron near the ion (i.e., for $z \lesssim r$). In unscaled variables, the high frequency components are of order v_e/r, where $m_e v_e^2 \sim e^2/r$, which when scaled is $v_e/(r_2\Omega_{ci}) = \sqrt{m_i/m_e}\tilde{r}^{-3/2}$. Thus, the criterion used in Sec. I is correct even for $\tilde{z}_{max} \gg \tilde{r}$.

Turning next to the requirement that the cross field motion be slow compared to the field aligned oscillations, we note first that the cross field motion affects the field aligned oscillations only through the time dependence in $r^2(t)$ [see Eq. (7)]. Thus, we examine the Poisson bracket

$$\frac{d\tilde{r}^2}{d\tilde{t}} = [\tilde{r}^2, \tilde{H}] = 2\tilde{y}(\tilde{t})\tilde{P}, \quad (30)$$

where $\tilde{H}$ is the scaled Hamiltonian (19).

The different trajectories in the figures of Sec. III are characterized by different time dependencies for $\tilde{y}(\tilde{t})$. Consider, for example, the three classes of trajectories in Fig. 4(a). For the trajectories that encircle the minimum value of $\tilde{H}$ at $\tilde{r}=0$, $\tilde{y}(\tilde{t})$ oscillates at the rotation frequency of the vector $\vec{r}(\tilde{t})$, which when scaled is $\omega_D/\Omega_{ci} = 1/\tilde{r}^3$. Equivalently, from Hamilton's equations we obtain $\partial \tilde{H}/\partial(\tilde{r}^2/2) \simeq \partial/\partial(\tilde{r}^2/2)(-1/\tilde{r}) = 1/\tilde{r}^3$.

Figure 4(a) is plotted for the case where $z_{max}=0$ and $\tilde{H}_z = -1/\tilde{r}$. For a case where $z_{max} \gg r$, such as the plots in Fig. 9, one can show that the rotation frequency is approximately

$$\frac{\partial \tilde{H}_z}{\partial(\tilde{r}^2/2)} \simeq \frac{1}{\tilde{r}^3}\xi^{3/2} = \frac{1}{\tilde{r}^{3/2}(z_{max}^2 + \tilde{r}^2)^{3/4}}. \quad (31)$$

For the trajectories in Fig. 4 that encircle the minimum in $\tilde{H}$ at finite $\tilde{p}_y$, the ion and electron $\vec{E} \times \vec{B}$ drift together, as shown in Fig. 2, but the ion also executes cyclotron motion in the drift frame. In unscaled variables $r(t)$ varies at the frequency Ω_{ci}, which corresponds to the scaled frequency $\Omega_{ci}/\Omega_{ci}=1$. One can easily check this result using the scaled Hamiltonian directly.

For the trajectories in Fig. 4 that encircle both minima, the scaled frequency of the motion is approximately $\Omega_{ci}/\Omega_{ci}=1$, but there can be high frequency components associated with the close passage of the ion near the electron (i.e., for small $\tilde{r}$). An estimate for the high frequency component is

$$\frac{1}{\tilde{r}^2}\frac{d\tilde{r}^2}{d\tilde{t}} = \frac{\tilde{y}\tilde{P}}{\tilde{r}^2} \lesssim \left(\frac{v_i}{r_2\Omega_{ci}}\right)\frac{1}{\tilde{r}} \lesssim \frac{1}{\tilde{r}^{3/2}}, \quad (32)$$

where $\tilde{r}$ is the minimum value of the cross field separation and we have assumed that $m_i v_i^2 \lesssim e^2/r$. The frequency of field aligned oscillations given in Eq. (27) must be large compared to the cross field frequencies, so we obtain the requirement

$$\sqrt{\frac{m_i}{m_e}}\frac{1}{(\tilde{r}^2+\tilde{z}^2)^{3/4}} \gg \frac{1}{\tilde{r}^{3/2}(\tilde{r}^2+\tilde{z}^2)^{3/4}}, 1, \frac{1}{\tilde{r}^{3/2}}. \quad (33)$$

The first term on the right is small compared to the term on the left provided that $\tilde{r} \gg (m_e/m_i)^{1/3}$, which is the same as inequality (29). This inequality (i.e., $r \gg r_2(m_e/m_i)^{1/3} = r_1$) is the basic requirement that the the binding be sufficiently weak.

The second term on the right is small compared to the term on the left provided that the binding is not too weak [i.e., $(\tilde{r}^2+\tilde{z}^2)^{1/2} \ll (m_i/m_e)^{1/3}$]. Thus, the allowed electron-ion separations are bounded below and above [i.e., $(m_e/m_i)^{1/3} \ll \tilde{r}$, $(\tilde{r}^2+\tilde{z}^2)^{1/2} \ll (m_i/m_e)^{1/3}$]. Even for an electron and proton, the ratio of the upper to the lower bound is large, $(m_i/m_e)^{2/3} \simeq 150$. Finally, the third term on the right is small compared to the term on the left provided the atom is not too elongated [i.e., $\tilde{z}_{max}/\tilde{r} \ll (m_i/m_e)^{1/3}$]. For applications such as to the weakly bound pairs in the ATRAP and ATHENA experiments the lower bound [i.e., $(m_e/m_i)^{1/3} < \tilde{r}$] is the constraint of primary concern.

As examples, we now examine numerical solutions of the full equations of motion for a case where the lower bound constraint is satisfied and a case where it is not satisfied. In Fig. 9, the dashed circle indicates the lower bound [i.e., $\tilde{r}=(m_e/m_i)^{1/3} \simeq 0.082$] for the case of electron-proton mass ratio. The upper bound is well outside the domain of the figure. The adiabatic invariants should be conserved for trajectories that lie completely outside the dashed circle.
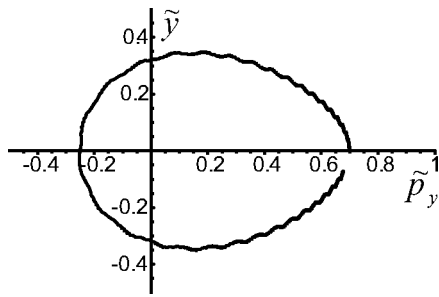
FIG. 12. Numerical solution of the equations of motion for the trajectory starting at $\vec{\tilde{r}}_e = (0,0,0)$, $\vec{\tilde{r}}_i = (0.7,0,0)$, $\vec{\tilde{v}}_e = (0,0,-39.297)$, $\vec{\tilde{v}}_i = (0,0.8,0.0213919)$, $m_i/m_e = 1837$; the electron is not treated in drift approximation (i.e., full dynamics in magnetic field for both particles).

Figure 12 shows a trajectory obtained by numerically solving the full equations of motion, including the cyclotron and z-bounce motion. As expected for a case where the actions are good invariants, the trajectory differs only slightly from the corresponding trajectory in Fig. 9. The small ripples on the trajectory in Fig. 12 are caused by the change in the drift velocity as the electron oscillates back and forth in z. Smaller and higher frequency oscillations caused by the electron-cyclotron motion are not visible in the figure.

In Fig. 10, the dashed circle again is drawn to indicate the lower bound, $\tilde{r} = (m_e/m_i)^{1/3}$. Figure 13 shows the result of a numerical solution of the full equations of motion for a trajectory that starts at $(\tilde{p}_y, \tilde{y}) = (0.26,0)$ and has values of $\sqrt{m_i/m_e}\tilde{I}_z$ and $\tilde{P}_Y$ corresponding to Fig. 10. For this trajectory $z_{max}/r \sim O(5-10)$ is rather large. The periodic helical excursions on the trajectory occur when the electron is near a turning point for the field aligned oscillations. The electron cyclotron motion combines with the slow ion velocity to produce the helical excursion. When the field aligned oscillation brings the electron near the ion again, the transverse electric field rises dramatically, and the electron steps to the next helical excursion. The combination of the excursions and the periodic electron steps produce a trajectory that loosely follows the trajectory in Fig. 10. However, the rapid
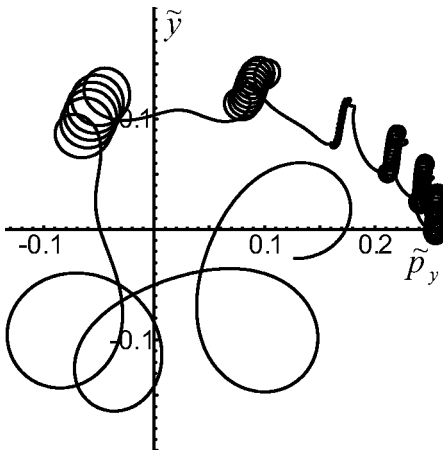
rise and fall of the transverse electric field breaks the adiabatic invariants, mixing axial and transverse kinetic energies. One can see in Fig. 10 that the size of the cyclotron radius varies from excursion to excursion gradually increasing.

V. BOHR–SOMMERFELD QUANTIZATION

Since the motion is quasiclassical, we introduce quantum numbers by using the Bohr–Sommerfeld rule, that is by quantizing the actions. Hamiltonian (16) includes the the cyclotron action and the action for field aligned oscillations, but the action for the cross field drift motion must still be introduced.

This action is obtained by solving Eq. (16) for $p_y = p_y(H - I_{ce}\Omega_{ce}, P_Y, I_z, y)$ and evaluating the integral

$$I_D = \frac{1}{2\pi} \oint p_y(H - I_{ce}\Omega_{ce}, P_Y, I_z, y) dy \qquad (34)$$

over a contour of constant H. I_D is simply $1/(2\pi)$ times the phase space area enclosed by the contour.

The quantization is effected by setting $I_D = \hbar n_D$, $I_z = \hbar n_z$, and $I_{ce} = \hbar(n_c + 1/2)$ in Eq. (34), where n_D, n_z, and n_c are integers. The 1/2 is retained in the quantization rule for the cyclotron motion since n_c may be relatively small. In principle, Eq. (34) can be inverted to find the system energy as a function of P_Y and the quantum numbers: $H = H(P_Y, n_c, n_z, n_D)$. the momentum P_Y is not quantized.

Fortunately, this prescription is easy to carry out in the most important limit: a guiding center drift atom with relatively tight binding. In this case the drift motion corresponds to that shown in Fig. 1. Equation (34) then reduces to the simple form

$$I_D = \frac{1}{2\pi} \oint p_y dy = \frac{1}{2\pi} \frac{eB}{c} \oint x dy = \frac{eB}{2\pi c} \pi r^2, \qquad (35)$$

where r is the radius of the nearly circular orbit. Quantizing the action I_D then yields the allowed radii,

$$r(n_D) = \sqrt{\frac{2\hbar n_D c}{eB}}. \qquad (36)$$

Substituting this expression and the quantized values of I_c and I_z into Hamiltonian (16) yields the allowed energies

$$H = \frac{P_Y^2}{2m_i} + \hbar\Omega_{ce}\left(n_c + \frac{1}{2}\right) - \frac{e^2}{r(n_D)}\Phi^{-1}\left[\frac{\hbar n_z}{e\sqrt{m_e r(n_D)}}\right]. \qquad (37)$$

In writing the kinetic energy for the ion as $P_Y^2/(2m_i)$, use was made of the fact that $r(n_D)$ is small (relatively tight binding). For the case where I_z also is small [i.e., $z_{max} \ll r(n_D)$], approximations (12) and (13) yield the further simplification

$$H = \frac{P_Y^2}{2m_i} + \hbar\Omega_{ce}\left(n_c + \frac{1}{2}\right) - \frac{e^2}{r(n_D)} + \hbar\omega_z[r(n_D)]n_z, \qquad (38)$$

where $\omega_z(r) = \sqrt{e^2/(m_e r^3)}$.

For small changes in the quantum numbers, the change in the energy is given by

FIG. 13. Numerical solution of the equations of motion for the trajectory starting at $\vec{\tilde{r}}_e = (0,0,0)$, $\vec{\tilde{r}}_i = (0.26,0,0)$, $\vec{\tilde{v}}_e = (0,0,-104.095)$, $\vec{\tilde{v}}_i = (0,1.24,0.056\,666)$, $m_i/m_e = 1837$; the electron is not treated in drift approximation (i.e., full dynamics in magnetic field for both particles).

$$\Delta H = \frac{\partial H}{\partial I_c}\hbar \Delta n_c + \frac{\partial H}{\partial I_z}\hbar \Delta n_z + \frac{\partial H}{\partial I_D}\hbar \Delta n_D, \qquad (39)$$

where $\partial H/\partial I_c = \Omega_{ce}$, $\partial H/\partial I_z = \omega_z$, and $\partial H/\partial I_D = \omega_D$. Thus, the energy level spacings for single integer changes in the quantum numbers (Δn_c, Δn_z, $\Delta n_D = 1$) are ordered as the frequencies [see inequality (1)]. Further, since the energies associated with the cyclotron motion, field aligned oscillations, and Coulomb interaction are comparable, the corresponding quantum numbers are ordered inversely to the frequencies (i.e., $n_c \ll n_z \ll n_D$).

We note that more accurate calculations would find corrections to $\partial H/\partial I_c$ that are of order $\partial H/\partial I_D = \omega_D$. However, these corrections contribute negligibly to the overall energy since $n_D \gg n_c$.

Finally, for a drifting pair with an electron orbit near the bottom of the outer well [see the small nearly circular orbit centered at ($y = 0$, $p_y \simeq P$) in Fig. 4]; the Hamiltonian may be Taylor expanded about the bottom of the well to obtain

$$H \simeq \Omega_{ce}I_{ce} + \omega_z I_z + \frac{1}{2}\frac{\partial^2 H}{\partial y^2}y^2 + \frac{1}{2}\frac{\partial^2 H}{\partial p_y^2}(p_y - p_y^{(0)})^2, \qquad (40)$$

where

$$\frac{\partial^2 H}{\partial y^2} = m_i \Omega_{ci}^2 - \frac{e^5 B^3}{c^3 (p_y^{(0)})^3},$$

$$\frac{\partial^2 H}{\partial p_y^2} = \frac{1}{m_i} - 2\frac{e^3 B^2}{c(p_y^{(0)})^3}, \qquad (41)$$

and $p_y^{(0)} \simeq P$ is the bottom of the well. Also, we have taken the simple case of small axial bounce motion and used Eq. (13). In this case, the Bohr–Sommerfeld quantization rules yield the energy levels

$$H \simeq \hbar \Omega_{ce}\left(n_c + \frac{1}{2}\right) + \hbar \omega_z n_z + \sqrt{\frac{\partial^2 H}{\partial y^2}\frac{\partial^2 H}{\partial p_y^2}}\hbar n_D. \qquad (42)$$

For our frequency ordering this expression reproduces results obtained previously using a quantum treatment for a quadratic aproximation to the outer well.[8]

VI. FIELD IONIZATION

Thus far, we have considered the case where the external electric field vanishes in the laboratory frame. As was mentioned earlier, the case of a uniform electric field directed transverse to the magnetic field is included implicitly through a change of reference frame, that is, a shift in the initial ion velocities, $\vec{v}_i(0) \rightarrow \vec{v}_i(0) - c\mathbf{E}\times\mathbf{B}/B^2$. However, such a shift cannot account for an electric field that is parallel to the magnetic field or an electric field that is spatially varying.

In the ATRAP experiments,[6] ionization of the guiding center drift atoms by an electric field (field ionization) was used to measure binding energies. For interpretation of such experiments, it would be useful to know the critical field for ionization as a function of the quantum numbers (or actions) for the atomic state.
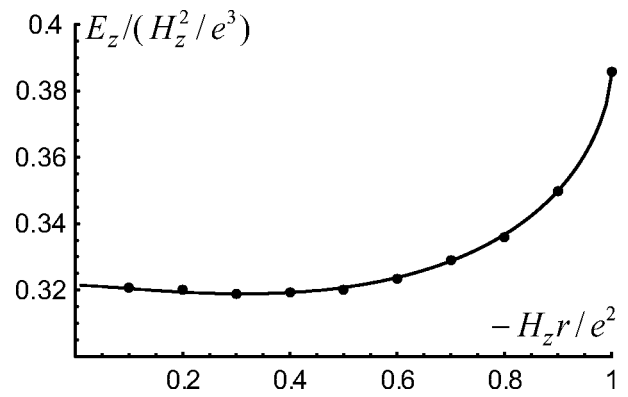

FIG. 14. Ionization by an electric field parallel to the magnetic field. E_z is the critical field for ionization, H_z is the initial binding energy before the atom enters the electric field, and r is the radius of the nearly circular initial drift orbit. The solid curve results from a theory based on constancy of I_z, and the points are solutions of Hamilton's equations of motion.

First consider the case where the electric field is parallel to the magnetic field and the atom is moving slowly up a gradient in the field. The binding energy in Eq. (7) is then replaced by

$$H_z = \frac{p_z^2}{2\mu} - \frac{e^2}{\sqrt{r^2 + z^2}} - eE_z(t)z, \qquad (43)$$

where $E_z(t) \equiv E[z_{\text{atom}}(t)]$ is the electric field at the location of the atom, and we have neglected the variation in the field over the dimensions of the atom. As the atom moves up the gradient in the field, H_z is not constant in time. Rather, the action,

$$I_z(H_z, E_z, r) = \frac{1}{2\pi}\oint p_z[H_z, E_z, r, z]dz, \qquad (44)$$

is constant until just before ionization. For simplicity, we consider tightly bound drift orbits with nearly circular orbits and neglect variation in r during the ionization process.

The electric field cannot increase indefinitely. At a certain critical value of $E_z(t)$, one of the turning points for the integral in Eq. (44) ceases to exist, the adiabatic invariant fails, and field ionization occurs. Implementing these ideas numerically yields the solid curve in Fig. 14: a plot of the scaled critical field, $E_z/(H_z^2/e^3)$, versus the scaled radius, $-H_z r/e^2$. Here, H_z is the initial binding energy, that is, the binding energy before the atom enters the electric field. Recall that H_z is related to I_z and r (or, the drift action $I_D = eBr^2/2c$) through Eq. (7). The limit $-H_z r/e^2 = 1$ corresponds to $I_z = 0$. In this limit, $E_z/(H_z^2/e^3)$ reaches the maximum value $2/3\sqrt{3}$. Although the full curve in Fig. 14 was obtained numerically, the maximum value can be obtained analytically. To check this theory, Hamilton's equations of motion were integrated forward in time through the field ionization event for various initial conditions. The results are shown as the points in Fig. 14. One can see that the theory based on constancy of I_z is accurate.

The scaling used in Fig. 14 provides a significant simplification. Without the scaling, the critical field would have to be written as a two-dimensional function, $E_z = f(H_z, r)$.

The scaling results from the fact that the Coulomb interaction does not introduce a separate length scale, so all lengths can be scaled in terms of e^2/H_z.

Next consider the case where an atom moves up a gradient in a transverse electric field. For a sufficiently weak gradient, the electric field can be treated as uniform over the dimensions of the atom, but slowly varying in time because of the motion of the atom. As mentioned, a uniform transverse field can be accounted for by a shift in ion velocity, or equivalently, a shift in the total transverse momentum

$$\mathbf{P} \to \mathbf{P}_{\text{eff}} = \mathbf{P}(t) - \frac{m_i c \mathbf{E}(t) \times \mathbf{B}}{B^2}, \tag{45}$$

where $\mathbf{E}(t)$ is the electric field at the location of the atom. We have also allowed for a slow time dependence in the atom momentum, $\mathbf{P}(t)$. The electric field polarizes the atom, and then the gradient in the field gives rise to a weak force on the atom and a slow time variation in the atom momentum. We will discuss this point later. Here, we need only realize that $\mathbf{P}_{\text{eff}}(t)$ changes slowly in time because of the atom motion.

Substituting $\mathbf{P}_{\text{eff}}(t)$ for $\mathbf{P}$ in Eq. (16), with P_x not set arbitrarily to zero, yields a Hamiltonian for the relative electron-ion motion, $\mathbf{r}(t)$. To understand the field ionization process, it is useful to refer again to Fig. 4(b). The peak in the effective potential separating the Coulomb well and the outer well moves to the left as $|\mathbf{P}_{\text{eff}}(t)|$ increases. Correspondingly, in Fig. 4(a) the x point in the separatrix moves to the left. We imagine that the atom starts with a nearly circular guiding center drift orbit inside the Coulomb well. As the atom moves up the gradient in the transverse electric field and $|\mathbf{P}_{\text{eff}}(t)|$ increases, the x point moves toward the orbit, and the orbit distorts from circularity. Eventually, the phase trajectory crosses the separatrix to the outer well. The atom becomes a drifting pair and is quickly ionized by the gradient. One can easily show that drifting pairs are always separated by a field gradient. Effectively, field ionization occurs when the trajectory crosses the separatrix.

During this process, the Hamiltonian is not a constant of the motion since $\mathbf{P}_{\text{eff}}(t)$ depends explicitly on time. However, the transverse action

$$I_D = \frac{1}{2\pi} \oint p_y[y, H, I_z, \mathbf{P}_{\text{eff}}(t)] dy \tag{46}$$

is nearly constant up to the separatrix crossing. The characteristic time for a drift cycle is small compared to the time scale on which $\mathbf{P}_{\text{eff}}(t)$ changes. The constancy of the actions, I_D and I_z, allows us to determine the critical $|\mathbf{P}_{\text{eff}}|$ for field ionization as a function of the initial values of the actions.

Figure 15 shows the result of a numerical implementation of these ideas for the simple case where $I_z = 0$. The abscissa and ordinate are scaled as in Sec. III. The ordinate is the scaled drift action $\tilde{I}_D = I_D / m_i \Omega_{ci} r_2^2 = \tilde{r}^2/2$, where $\tilde{r} = r/r_2$ is the scaled radius of the nearly circular initial drift orbit. Rather than referring to a critical effective momentum for ionization, we refer to a critical effective electric field, $E_{\text{eff}} \equiv |\mathbf{P}_{\text{eff}} \times \mathbf{B}/m_i c|$. The abscissa in Fig. 15 is the scaled critical field, $\tilde{E}_{\text{eff}} = E_{\text{eff}}/(e/r_2^2)$. The critical field is always
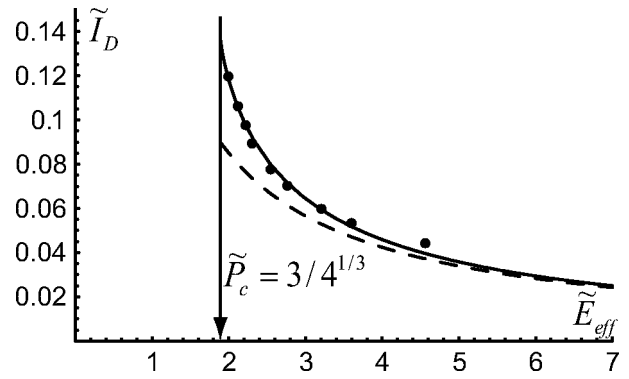

FIG. 15. Ionization by an effective electric field transverse to the magnetic field for the simple case where the bounce action is zero (i.e., $I_z = 0$). The effective field $\tilde{E}_{\text{eff}} = E_{\text{eff}}/(e/r_2^2)$ and the drift action $\tilde{I}_D = \tilde{r}^2/2$ are scaled as in Sec. III. The solid curve results from a theory based on the constancy of I_D and the points from the solution of the coupled electron-ion equations of motion. The dashed curve is an approximate analytic solution, $\tilde{E}_{\text{eff}} \simeq \chi/\tilde{I}_D$, that assumes tight binding ($\tilde{r}^3 \ll 1$). The arrow at $\tilde{E}_{\text{eff}} = \tilde{P}_c = 3/4^{1/3}$ (see Fig. 5 for the definition of $\tilde{P}_c$) limits the range of possible field ionization.

larger than the momentum at which the outer well disappears (i.e., $\tilde{E}_{\text{eff}} = |\tilde{\mathbf{P}}_{\text{eff}}| > \tilde{P}_c = 3/4^{1/3}$, see Fig. 5). The solid curve in Fig. 15 results from the theory based on constancy of the adiabatic invariants, and the points are from numerical solutions of the coupled electron-ion equations and equations of motion.

For the case of sufficiently tight initial binding (i.e., $\tilde{r}^3 \ll 1$), an analytic expression can be obtained for the scaled critical field

$$\tilde{E}_{\text{eff}} \simeq \chi/I_D = 2\chi/\tilde{r}^2, \tag{47}$$

where

$$\chi = \frac{1}{\pi} [\sqrt{2} + \ln(2 + 2^{3/2}) - 2 \ln(2 + \sqrt{2})] \simeq 0.17. \tag{48}$$

This approximate result is shown in the dashed curve in Fig. 15.

We emphasize that the effective electric field, $\tilde{\mathbf{E}}_{\text{eff}} = \tilde{\mathbf{E}}(t) + \tilde{\mathbf{P}}(t) \times \hat{z}$, depends on both the lab-frame electric field and the atom momentum. Moreover, a gradient in the electric field gives rise to a force on the polarized atom and changes its momentum. In a subsequent paper we will discuss the motion of the atom under this force. Here, we simply note that the change in the effective field due to the change in the atom momentum is small for sufficiently tight binding (i.e., for $\tilde{r}^3 \ll 1$).

ACKNOWLEDGMENTS

Phys. Plasmas, Vol. 11, No. 5, May 2004

Guiding center drift atoms   2393

[1]M.E. Glinsky and T.M. O'Neil, Phys. Fluids B **3**, 1279 (1991).

[2]S. Saini and D. Farrelly, Phys. Rev. A **36**, 3556 (1987).

[3]L.D. Landau and E.M. Lifshtz, *Quantum Mechanics: Non-relativistic Theory* (Pergamon, New York, 1977), p. 461.

[4]M. Amoretti, C. Amsler, G. Bonomi *et al.*, Nature (London) **419**, 456 (2002).

[5]G. Gabrielse, N.S. Bowden, P. Oxley *et al.*, Phys. Rev. Lett. **89**, 213401 (2002).

[6]G. Gabrielse, N.S. Bowden, P. Oxley *et al.*, Phys. Rev. Lett. **89**, 233401 (2002).

[7]J.E. Avron, I.W. Herbst, and B. Simon, Ann. Phys. (N.Y.) **114**, 431 (1978).

[8]O. Dippel, P. Schmelcher, and L.S. Cederbaum, Phys. Rev. A **49**, 4415 (1994).

[9]J. Shertzer, J. Ackermann, and P. Schmelcher, Phys. Rev. A **58**, 1129 (1998).